J. Fluid Mech. (1966), *vol.* 24, *part* 3, *pp.* 555–575
Printed in Great Britain

Viscous stratified flow towards a sink

By ROBERT C. Y. KOH
W. M. Keck Laboratory of Hydraulics and Water Resources,
California Institute of Technology

(Received 8 December 1964)

In this paper the viscous, slightly stratified flow towards a sink is investigated. The fluid is assumed incompressible, linearly stratified in density, and the flow steady. The theoretical portion of this paper includes both the two-dimensional and the axisymmetric cases, whereas the experimental portion includes only the two-dimensional case. The solutions obtained indicate that there exists a withdrawal layer symmetrically situated about the horizontal plane of the sink. The flow occurs in this layer while outside this layer there is essentially no motion. This withdrawal layer grows in thickness with the distance x (or r) from the sink at a rate proportional to $x^{\frac{1}{3}}$ (or $r^{\frac{1}{3}}$). The velocity distributions $u(y)$ (or $u(z)$) are similar from one station x (or r) to another.

1. Theoretical investigations

1.1. *Introduction*

Weak motions of a density-stratified fluid in a gravitational field often exhibit large departures from the motion of homogeneous fluids. Physically, in a stably stratified fluid, work must be done to displace any fluid particle vertically since there is a force due to the gravity field always tending to oppose the displacement. Vertical motions are therefore inhibited in favour of horizontal motion. Stratified flows are common in the oceans and in the atmosphere.

The problem of linearly stratified flow towards a sink was first investigated by Yih (1958) for the two-dimensional inviscid case. The fluid is assumed to occupy a semi-infinite rectangular strip with the sink located at the lower corner of the end of the strip as shown in figure 1. He assumed that the velocity distribution at infinity is such that

$$\rho U^2 = \text{const.},$$

where ρ is the density and U the horizontal velocity, both functions of the vertical co-ordinate y. The solution is found expressed in a Fourier series for values of the internal Froude number $F = U/d(g\epsilon)^{\frac{1}{2}}$ greater than $1/\pi$ where d is the depth, ϵ the density gradient and g the gravitational acceleration. For internal Froude numbers less than $1/\pi$, the solution exhibits waves and thus the assumption on the velocity distribution at infinity is no longer justified. Kao (1963) extended Yih's solution to include cases where the internal Froude number is less than $1/\pi$ by introducing a uniform sink distribution on the vertical wall as shown in figure 2. The flow field would then possess a dividing streamline above which the fluid leaves by way of the distributed sink and below which the fluid comes out of

the bottom sink. By requiring that the pressure on this dividing streamline be equivalent to the hydrostatic pressure due to the fluid above it, the flow above the dividing streamline may be replaced by stagnant fluid with a vortex sheet at the dividing streamline. The conclusion is that the internal Froude number based on the height of the dividing streamline at infinity is equal to a constant 0·345.

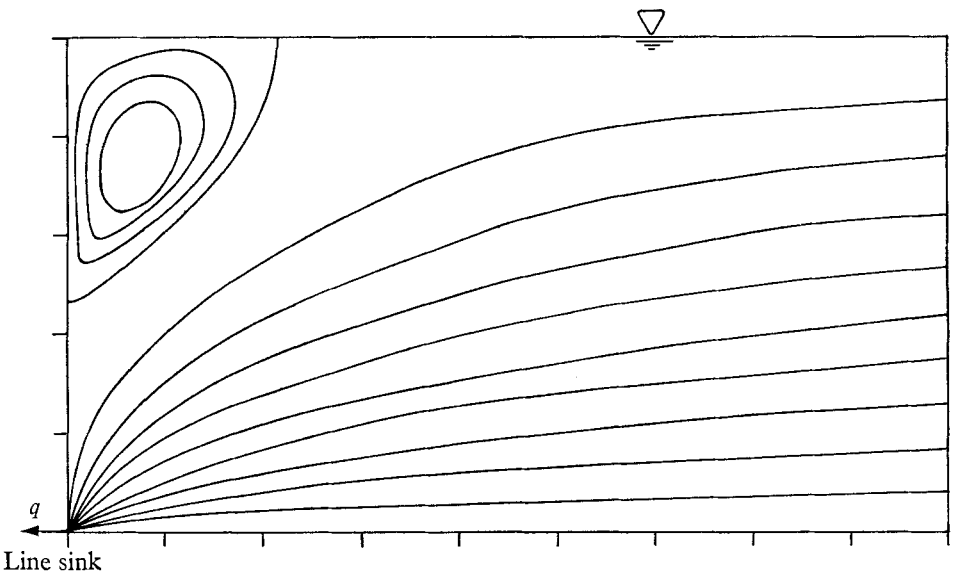

FIGURE 1. Yih's solution for $F = 0{\cdot}35$. Lines shown are streamlines (from Yih 1958).

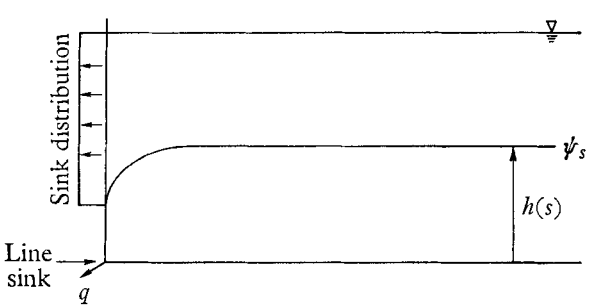

FIGURE 2. Kao's method of solution.

Debler (1959) and Gariel (1949) both performed experiments on linearly stratified flow towards a sink. Because of the inherent difficulty in making steady experiments with continuously stratified flows, the results are not very conclusive. Only the gross quantities such as discharge, thickness of the withdrawal layer, and density gradient were measured.

It is interesting to investigate the effect of viscosity in stratified flow towards a sink especially since the motion usually has to be weak for the stratification to be important. Little work has been done in the field of viscous, continuously stratified flow. Long (1962) investigated the problem of the flow over and behind

a flat plate in a viscous, linearly stratified flow by linearizing the equations. A similar approach is used here to solve the problem of the viscous stratified flow towards a sink. A perturbation-similarity procedure is developed from which the relative importance of the neglected terms may be clearly seen.

Experiments were performed in a laboratory tank and the results compared with the analytical solution. These experiments will be discussed in § 2 of this paper.

The work reported herein is a condensed version of a thesis (1964) submitted by the author in partial fulfilment of the degree of Doctor of Philosophy.

1.2. *Formulation of the equations*

Consider an incompressible, slightly stratified fluid occupying all space. A hydrodynamic sink is located at the origin and withdraws the fluid at a rate q. The two-dimensional case will be treated in detail here. The axisymmetric case will be summarized later on in this paper, while the detailed developments will be omitted.

The continuity equation for pure fluid flow is

$$\nabla.(\rho\mathbf{u}) + \partial\rho/\partial t = 0, \tag{1.1}$$

where $\mathbf{u}$ is the velocity vector, ρ the density, t the time, and $\nabla.$ the divergence operator. If the fluid is stratified and the stratification is due to temperature variations alone, then equation (1.1) is the continuity equation for the flow. If, however, there is a foreign substance in the fluid such as dissolved salts in water, then there is the additional transfer of mass due to molecular diffusion of the salt through the water and the full continuity equation should read

$$\frac{\partial\rho}{\partial t} + \nabla.(\rho\mathbf{u}) = \nabla.(D\nabla c), \tag{1.2}$$

where D is the molecular diffusion coefficient, and c the concentration of the salt. It may be readily deduced, to the order of approximation $\Delta\rho/\rho_0$ (where $\Delta\rho$ is the total change in density in the relevant flow field, and ρ_0 is the density at the level of the sink), that the continuity equation (1.1) may be written as

$$\frac{1}{\rho}\frac{\partial\rho}{\partial t} + \nabla.\mathbf{u} = 0. \tag{1.3}$$

For steady flow, it becomes simply

$$\nabla.\mathbf{u} = 0. \tag{1.4}$$

The equation of state for the flow of an ordinary incompressible fluid is, of course,

$$\rho = \text{const.}$$

For a stratified fluid, the continuity equation for the substance or agent responsible for the stratification and a relation between the concentration of this agent and the density must be considered. Such a relation would, in general, be

$$\frac{dc}{dt} = \frac{\partial c}{\partial t} + \mathbf{u}.\nabla c = \nabla.(D\nabla c), \tag{1.5}$$

where, if the stratification is thermal, D would be the thermal diffusivity and c the temperature. We next assume that the relation between c and ρ is linear. Thus

$$\rho - \rho_0 = k(c - c_0). \tag{1.6}$$

Combination of equations (1.5) and (1.6) gives

$$\frac{d\rho}{dt} = \nabla.(D\nabla\rho). \tag{1.7}$$

The general momentum equation may be written as

$$\rho \frac{d\mathbf{u}}{dt} + \nabla p = \nabla.\tau + \rho\mathbf{G}, \tag{1.8}$$

where $\mathbf{G}$ is the external force field, τ the stress tensor, and p the pressure.

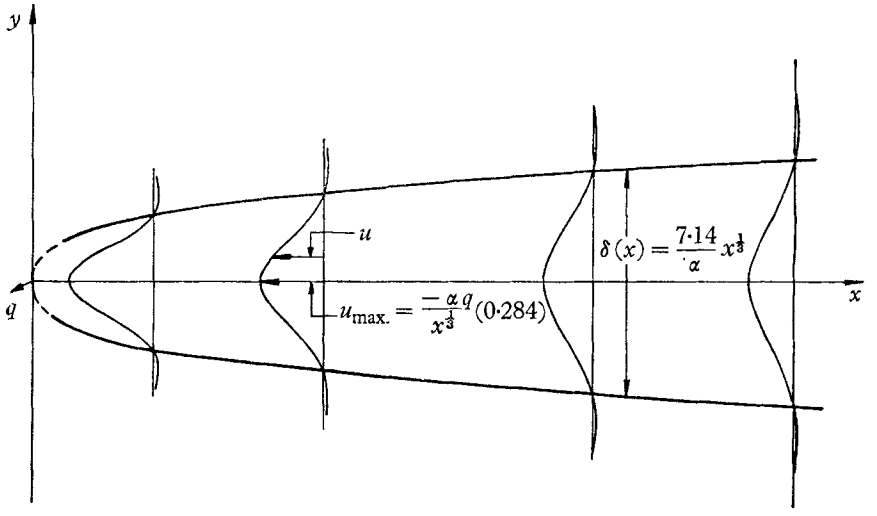

FIGURE 3. Viscous stratified flow towards a line sink: the withdrawal layer.

For a Newtonian fluid with first and second viscosity coefficients μ and λ in a gravitational field, equation (1.8) becomes

$$\rho \frac{d\mathbf{u}}{dt} + \nabla p = \mu\nabla^2\mathbf{u} + (\nabla\mu)[\nabla\mathbf{u} + (\nabla\mathbf{u})^*] + \rho[-g\mathbf{j}] + \nabla.(\lambda I \nabla.\mathbf{u}). \tag{1.9}$$

For steady, slightly stratified flow, by virtue of equation (1.4), it becomes

$$\rho \frac{d\mathbf{u}}{dt} + \nabla p = \mu\nabla^2\mathbf{u} + (\nabla\mu)[\nabla\mathbf{u} + (\nabla\mathbf{u})^*] + \rho[-g\mathbf{j}]. \tag{1.10}$$

1.3. *Boundary-layer assumption and the reduced equations*

Equations (1.4), (1.7), and (1.10) will now be applied to the problem of two-dimensional, steady, slightly but linearly stratified flow towards a sink at the origin. Rectangular co-ordinates x and y will be adopted as shown in figure 3. It will be assumed also that the fluid occupies all the right half plane but that, even though the flow field is infinite in extent, the bulk of the motion occurs

within a withdrawal layer (like a boundary layer) whose thickness $\delta(x)$ is much smaller than the distance x from the sink. The flow field and the velocity distributions might be as illustrated in figure 3.

Equations (1.4), (1.7), and (1.10) hence reduce to

$$\frac{\partial u}{\partial x}+\frac{\partial v}{\partial y}=0, \tag{1.11}$$

$$\rho\left[u\frac{\partial u}{\partial x}+v\frac{\partial u}{\partial y}\right]+\frac{\partial p}{\partial x}=\frac{\partial}{\partial y}\left(\mu\frac{\partial u}{\partial y}\right), \tag{1.12}$$

$$\frac{\partial p}{\partial y}=-\rho g, \tag{1.13}$$

$$u\frac{\partial \rho}{\partial x}+v\frac{\partial \rho}{\partial y}=D\frac{\partial^2 \rho}{\partial y^2}, \tag{1.14}$$

where u and v are the components of velocity in the x- and y-directions respectively. Terms of the order $\delta(x)/x$ and higher have been neglected and D is assumed to be constant. We introduce the stream function ψ such that

$$u=\partial\psi/\partial y, \quad v=-\partial\psi/\partial x. \tag{1.15}$$

We also define the density and viscosity perturbations as

$$\rho(x,y)=\rho_0+s_0(y)+s(x,y), \tag{1.16}$$

$$\mu(x,y)=\mu_0+\theta_0(y)+\theta(x,y), \tag{1.17}$$

where ρ_0 is the density of the undisturbed fluid at the sink level, μ_0 the viscosity of the undisturbed fluid at the sink level, $\rho_0+s_0(y)$ the density distribution if there were no motion, and $\mu_0+\theta_0(y)$ the viscosity distribution if there were no motion. Substituting equations (1.15), (1.16), and (1.17) into equations (1.12), (1.13), and (1.14), eliminating the pressure terms and remembering that

$$\left|\frac{s_0+s}{\rho_0}\right|\ll 1, \tag{1.18}$$

and

$$\left|\frac{\theta_0+\theta}{\mu_0}\right|\ll 1, \tag{1.19}$$

from the assumption of small stratifications, we obtain the two equations

$$\frac{\partial\psi}{\partial y}\frac{\partial s}{\partial x}-\frac{\partial\psi}{\partial x}\frac{\partial s}{\partial y}=D\left\{\frac{d^2 s_0}{dy^2}+\frac{\partial^2 s}{\partial y^2}\right\}+\frac{ds_0}{dy}\frac{\partial\psi}{\partial x}, \tag{1.20}$$

and

$$g\frac{\partial s}{\partial x}+\mu_0\frac{\partial^4\psi}{\partial y^4}=\rho_0\frac{\partial}{\partial y}\left\{\frac{\partial\psi}{\partial y}\frac{\partial^2\psi}{\partial x\,\partial y}-\frac{\partial\psi}{\partial x}\frac{\partial^2\psi}{\partial y^2}\right\}. \tag{1.21}$$

Before normalizing the equations, it is convenient to specify the parent density distribution. Assume that the hydrostatic density distribution is linear:

$$s_0(y)=-\epsilon\rho_0 y, \tag{1.22}$$

where

$$\epsilon=-\frac{1}{\rho_0}\frac{ds_0}{dy}=\text{const.}, \tag{1.23}$$

We define the following non-dimensional variables

$$\left.\begin{aligned} \phi &= \psi/q, \\ \eta &= \epsilon y, \\ \xi &= (\epsilon^3/\alpha_0^3)x, \\ \sigma &= (g/\rho_0 q \epsilon \nu \alpha_0^3)s, \end{aligned}\right\} \tag{1.24}$$

and also define the two parameters

$$\alpha_0^6 = \epsilon g/D\nu, \quad \beta = q\epsilon^2/\alpha_0^3 D.$$

Then equations (1.20) and (1.21) become

$$\frac{\partial^2\sigma}{\partial\eta^2} - \frac{\partial\phi}{\partial\xi} = \beta\left\{\frac{\partial\phi}{\partial\xi}\frac{\partial\sigma}{\partial\eta} - \frac{\partial\phi}{\partial\eta}\frac{\partial\sigma}{\partial\xi}\right\}, \tag{1.25}$$

$$\frac{\partial^4\phi}{\partial\eta^4} + \frac{\partial\sigma}{\partial\xi} = \frac{D}{\nu}\beta\left\{\frac{\partial\phi}{\partial\eta}\frac{\partial^3\phi}{\partial\xi\,\partial\eta^2} - \frac{\partial\phi}{\partial\xi}\frac{\partial^3\phi}{\partial\eta^3}\right\}. \tag{1.26}$$

The boundary conditions expressed in the non-dimensional variables are

$$\int_{-\infty}^{\infty}\frac{\partial\phi}{\partial\eta}\,d\eta = -1, \tag{1.27}$$

$$\sigma, \frac{\partial\phi}{\partial\xi}, \frac{\partial\phi}{\partial\eta}, \frac{\partial^2\phi}{\partial\eta^2} \to 0 \quad \text{as} \quad \eta \to \pm\infty, \xi > 0, \tag{1.28}$$

$$\sigma \to 0 \quad \text{as} \quad \xi \to \infty. \tag{1.29}$$

1.4. *Solution to the two-dimensional problem*

To solve equations (1.25) and (1.26) subject to the conditions (1.27), (1.28) and (1.29), we assume a perturbation-similarity solution of the form

$$\phi(\xi,\eta) = f_0(\zeta) + \frac{\beta}{\xi^{\frac{2}{3}}}f_1(\zeta) + \left(\frac{\beta}{\xi^{\frac{2}{3}}}\right)^2 f_2(\zeta) + \ldots, \tag{1.30}$$

$$\sigma(\xi,\eta) = \frac{1}{\xi^{\frac{1}{3}}}\left\{h_0(\zeta) + \frac{\beta}{\xi^{\frac{2}{3}}}h_1(\zeta) + \left(\frac{\beta}{\xi^{\frac{2}{3}}}\right)^2 h_2(\zeta) + \ldots\right\}, \tag{1.31}$$

where

$$\zeta = \eta/\xi^{\frac{1}{3}} = \alpha_0 y/x^{\frac{1}{3}}, \tag{1.32}$$

and substitute them into the equations (1.25) and (1.26). Assuming $\beta/\xi^{\frac{2}{3}} \ll 1$, the various terms may be grouped according to their order. The net results are:

(i) To zeroth order

$$\frac{d^2h_0}{d\zeta^2} + \frac{\zeta}{3}\frac{df_0}{d\zeta} = 0, \tag{1.33}$$

$$\frac{d^4f_0}{d\zeta^4} - \frac{1}{3}\left\{\zeta\frac{dh_0}{d\zeta} + h_0\right\} = 0, \tag{1.34}$$

with the boundary conditions

$$\int_{-\infty}^{\infty}\frac{df_0}{d\zeta}\,d\zeta = -1, \tag{1.35}$$

$$h_0, \frac{df_0}{d\zeta}, \frac{d^2f_0}{d\zeta^2} \to 0 \quad \text{as} \quad \zeta \to \pm\infty. \tag{1.36}$$

(ii) To first order

$$\frac{d^2h_1}{d\zeta^2}+\frac{1}{3}\left\{\zeta\frac{df_1}{d\zeta}+2f_1\right\}=-\tfrac{1}{3}h_0\frac{df_0}{d\zeta}, \tag{1.37}$$

$$\frac{d^4f_1}{d\zeta^4}-\frac{1}{3}\left\{\zeta\frac{dh_1}{d\zeta}+3h_1\right\}=-\frac{2}{3}\frac{D}{\nu}\frac{df_0}{d\zeta}\frac{d^2f_0}{d\zeta^2}, \tag{1.38}$$

with the homogeneous boundary conditions

$$\int_{-\infty}^{\infty}\frac{df_1}{d\zeta}d\zeta=0, \tag{1.39}$$

$$h_1,\frac{df_1}{d\zeta},\frac{d^2f_1}{d\zeta^2}\to 0 \quad \text{as} \quad \zeta\to\pm\infty. \tag{1.40}$$

Similarly, one may obtain the equations for h_2, f_2, etc. although these will not be given here. In fact only the zeroth-order equations will be solved in detail. Solutions for h_1, f_1, etc., are solely a case of numerical analysis. The purpose of the perturbation analysis is primarily to show the effect of the neglected quantities. Note that the perturbation parameter is $\beta/\xi^{\frac{2}{3}}$ which is inversely proportional to the $\frac{2}{3}$ power of the distance from the sink. Thus the greater the distance from the sink, the better the approximation.

The equations (1.33) and (1.34) subject to the conditions (1.35) and (1.36) were solved numerically on an IBM 7090 computer. The solutions are shown graphically in figure 4. From figure 4, the velocity distribution may easily be visualized. The flow field indeed looks like the one shown in figure 3 with the withdrawal layer growing in thickness as $x^{\frac{1}{3}}$. If one defines δ as the thickness of the forward flow, then from figure 4

$$\delta(x)=7{\cdot}14x^{\frac{1}{3}}/\alpha_0. \tag{1.41}$$

The significance of the boundary-layer assumption may now be readily seen. From equation (1.41),

$$\frac{\delta}{x}=\frac{7{\cdot}14}{\alpha_0 x^{\frac{2}{3}}}. \tag{1.42}$$

For large x, δ/x may be made as small as one pleases provided α_0, which is proportional to the sixth root of the density gradient, is not zero. The validity of the boundary-layer assumption thus depends on both x and α_0.

The other parameters assumed small for the validity of the solution are: $q/D\alpha_0 x^{\frac{2}{3}}$, which is the perturbation parameter; $q/\nu\alpha_0 x^{\frac{2}{3}}$, which occurs disguised as D/ν in the first-order equations; and $\epsilon\delta$, which is the total relative change in density in the relevant flow field.

1.5. *The axisymmetric case*

For the axisymmetric case, let Q be the discharge, r be the horizontal radial co-ordinate and z be the vertical co-ordinate; we would have, instead of equations (1.20) and (1.21), the following equations:

$$D\left\{\frac{d^2s_0}{dz^2}+\frac{\partial^2 s}{\partial z^2}\right\}+\frac{1}{r}\frac{ds_0}{dz}\frac{\partial\psi}{\partial r}=\frac{1}{r}\left\{\frac{\partial\psi}{\partial z}\frac{\partial s}{\partial r}-\frac{\partial\psi}{\partial r}\frac{\partial s}{\partial z}\right\}, \tag{1.43}$$

$$g\frac{\partial s}{\partial r}+\frac{\mu_0}{r}\frac{\partial^4\psi}{\partial r^4}=\frac{\rho_0}{r^2}\frac{\partial}{\partial z}\left\{\frac{\partial\psi}{\partial z}\frac{\partial^2\psi}{\partial z\partial r}-\frac{\partial\psi}{\partial r}\frac{\partial^2\psi}{\partial z^2}-\frac{1}{r}\left(\frac{\partial\psi}{\partial z}\right)^2\right\}, \tag{1.44}$$

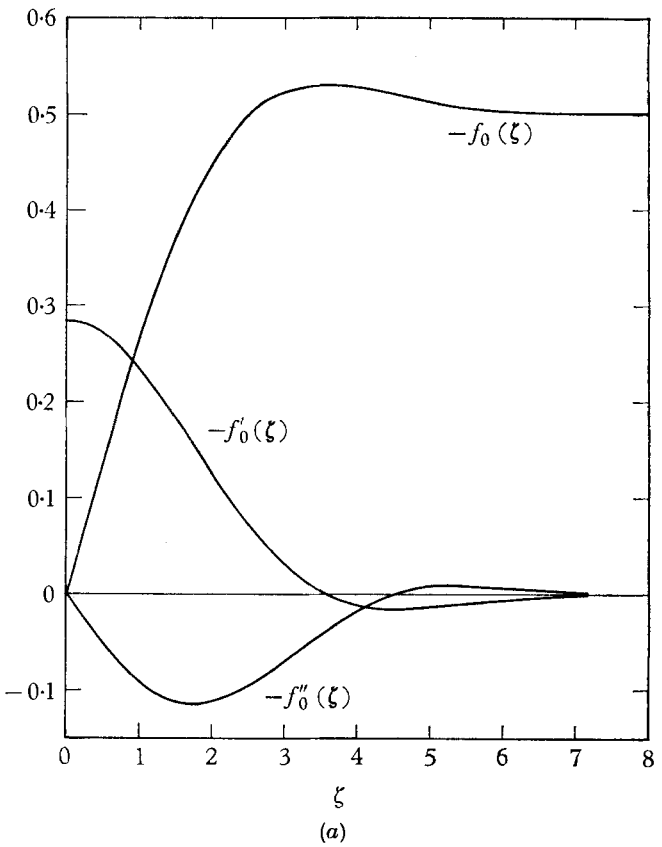

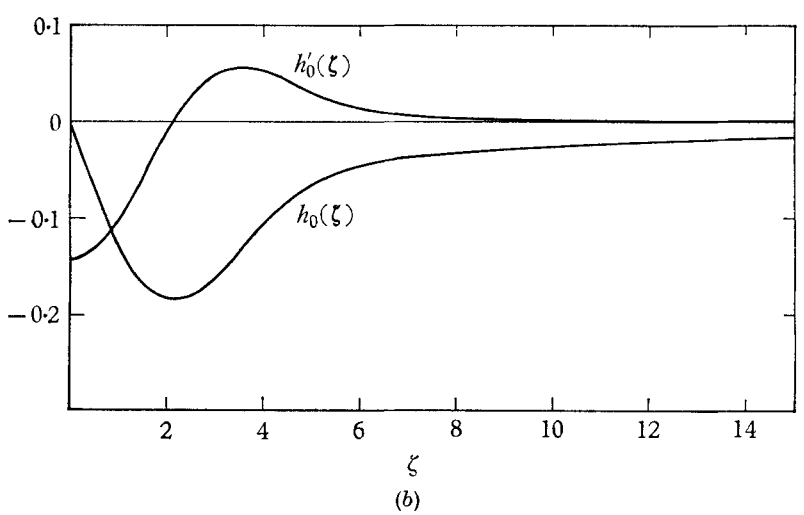

FIGURE 4. (*a*) The non-dimensional stream function and its derivatives for the two-dimensional case. (*b*) The non-dimensional density function and its first derivative for the two-dimensional case.

where ψ is the axisymmetric stream function and the other symbols have the same meaning as before. With the normalizations

$$\left.\begin{aligned} \phi &= \psi/(Q/2\pi), \quad \eta = \epsilon z, \\ \xi &= (\epsilon^3/\alpha_0^3) r, \quad \sigma = (2\pi g/\rho_0 \nu Q \epsilon^4) s, \end{aligned}\right\} \tag{1.45}$$

and defining $\beta = Q\nu\epsilon^4/2\pi g$, these equations may be written as

$$\frac{\partial^2\sigma}{\partial\eta^2} - \frac{1}{\xi}\frac{\partial\phi}{\partial\xi} = \left(\frac{Q\nu\epsilon^4}{2\pi g}\right)\frac{1}{\xi}\left\{\frac{\partial\phi}{\partial\eta}\frac{\partial\sigma}{\partial\xi} - \frac{\partial\sigma}{\partial\eta}\frac{\partial\phi}{\partial\xi}\right\}, \tag{1.46}$$

$$\frac{1}{\xi}\frac{\partial^4\phi}{\partial\eta^4} + \frac{\partial\sigma}{\partial\xi} = \frac{D}{\nu}\beta\frac{1}{\xi^2}\left\{\frac{\partial\phi}{\partial\eta}\frac{\partial^3\phi}{\partial\xi\,\partial\eta^2} - \frac{\partial\phi}{\partial\xi}\frac{\partial^3\phi}{\partial\eta^3} - \frac{2}{\xi}\frac{\partial\phi}{\partial\eta}\frac{\partial^2\phi}{\partial\eta^2}\right\}. \tag{1.47}$$

The boundary conditions are the same as before. Substitution of the perturbation-similarity series

$$\phi(\xi,\eta) = f_0(\zeta) + \frac{\beta}{\xi^{\frac{5}{3}}} f_1(\zeta) + \left(\frac{\beta}{\xi^{\frac{5}{3}}}\right)^2 f_2(\zeta) + \ldots, \tag{1.48}$$

$$\sigma(\xi,\eta) = \frac{1}{\xi^{\frac{4}{3}}}\left\{h_0(\zeta) + \frac{\beta}{\xi^{\frac{5}{3}}} h_1(\zeta) + \left(\frac{\beta}{\xi^{\frac{5}{3}}}\right)^2 h_2(\zeta) + \ldots\right\}, \tag{1.49}$$

into equations (1.46) and (1.47), assuming $\beta/\xi^{\frac{5}{3}} \ll 1$ and collecting terms of the same order, for the zeroth order we obtain

$$\frac{d^2h_0}{d\zeta^2} + \frac{\zeta}{3}\frac{df_0}{d\zeta} = 0, \tag{1.50}$$

$$\frac{d^4f_0}{d\zeta^4} - \frac{1}{3}\left\{\zeta\frac{dh_0}{d\zeta} + 4h_0\right\} = 0. \tag{1.51}$$

The boundary conditions are, of course, still given by equations (1.35) and (1.36). Higher-order equations may similarly be found although the details will not be given here. The solution to equations (1.50) and (1.51) is presented in figure 5.

It may be readily seen by comparison that the two-dimensional and the axisymmetric cases are very similar to each other. If one replaces x by r, y by z, q by $Q/2\pi r$, in the two-dimensional solution, one would have a good approximation to the axisymmetric solution. The thickness of the withdrawal layer is a little thinner being

$$\delta(r) = 5{\cdot}8r^{\frac{1}{3}}/\alpha_0$$

compared with

$$\delta(x) = 7{\cdot}14x^{\frac{1}{3}}/\alpha_0$$

for the two-dimensional case.

1.6. *Discussion of the validity of the theoretical solution*

The discussion in this section is only on the two-dimensional solution since this is the case which will be compared with the experiments later. Essentially the same discussion may be applied to the axisymmetric case because of the similarity discussed in the last paragraph of the previous section.

The analytical solution for the two-dimensional case (figure 4) is valid provided the four quantities $\epsilon\delta$, δ/x, $q/D\alpha_0x^{\frac{2}{3}}$, and $q/\nu\alpha_0x^{\frac{3}{3}}$ are all much smaller than unity.

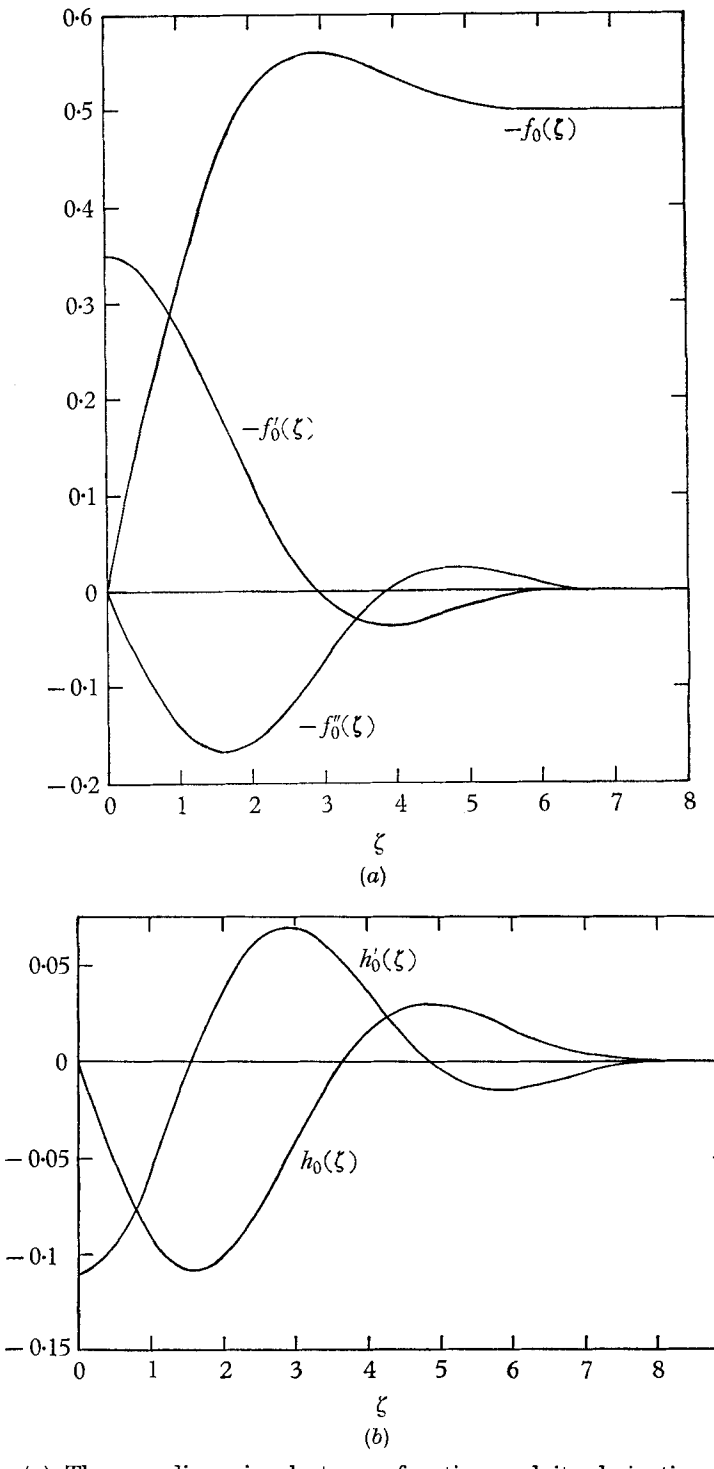

FIGURE 5. (*a*) The non-dimensional stream function and its derivatives for the axisymmetric case. (*b*) The non-dimensional density function and its first derivative for the axisymmetric case.

The first quantity $\epsilon\delta$ is the total relative change in density from the top to the bottom of the relevant flow field (in other words, the withdrawal layer). Since δ grows with x, the quantity $\epsilon\delta$ will be small when ϵ is very small and δ not very large. This means that the solution should not be applied when x is too large since δ would then be too large. From the solution, $\delta/x \propto 1/\alpha_0 x^{\frac{2}{3}}$. Thus, $\epsilon\delta \propto \epsilon x^{\frac{1}{3}}/\alpha_0$ must be $\ll 1$.

The second quantity δ/x is, by virtue of the solution, the same order as $1/\alpha_0 x^{\frac{2}{3}}$. For $\alpha_0 \neq 0$, this may be made very small when x is large.

The third and fourth quantities $q/D\alpha_0 x^{\frac{2}{3}}$, $q/\nu\alpha_0 x^{\frac{2}{3}}$ are very small when q is very small. The solution is taken to be the limiting solution when $q \to 0$. Thus, as long as D, ν, α_0, and x are not zero, these two parameters are truly negligible for small enough q.

Thus, to summarize the limitations imposed by the various assumptions on the validity of the theoretical solution, one may apply the zeroth-order solution if ϵ is very small, x is neither small nor exceedingly large, and q very small. In a given problem in the stratified flow towards a line sink, one would be given ϵ, q, D, ν, and hence α_0. One can then calculate the quantities $1/\alpha_0 x^{\frac{2}{3}}$, $q/D\alpha_0 x^{\frac{2}{3}}$, $q/\nu\alpha_0 x^{\frac{2}{3}}$, and $\epsilon x^{\frac{1}{3}}/\alpha_0$ for various x. For those values of x where all these quantities are small, the zeroth-order solution may be applied provided no further complications such as turbulence, non-linear density distribution, and complicated geometry come into the problem. The validity of the theoretical solution is thus confined to a range of the variable x, that range within which the four quantities above are very small. In any given case, the extent of this region may be very large or there may not be any value of x at which the solution is valid. It all depends on the magnitude of the parameters q, D, ν, and ϵ.

The analytical solution for the axisymmetric case (figure 5) is valid provided the quantities $\epsilon\delta$, δ/r, $Q/D\alpha_0 x^{\frac{5}{3}}$, $Q/\nu\alpha_0 x^{\frac{5}{3}}$ are all much smaller than unity.

2. Experimental investigations

To supplement the analytical solution, a series of experiments was performed in which fluid was withdrawn from a slit in the side of a tank filled with a linearly stratified liquid. This corresponds to the two-dimensional case discussed in § 1 of this paper.

In these experiments, density gradients were achieved in two different ways: (i) by means of a temperature gradient (designated as T-series runs), (ii) by means of dissolved salt (N-series runs).

2.1. *Apparatus and procedure*

The experimental reservoir was a long tank constructed of clear Lucite, $\frac{3}{8}$ in. thick. A schematic drawing of the reservoir is shown in figure 6. It is 45 cm deep, 250 cm long and 26 cm wide with a milk-white Lucite partition in the middle along the length of the tank extending from one end to a point 13 cm from the opposite end. This partition essentially doubles the length of the reservoir. On the discharge end was a slit 0·15 cm wide located 16 cm from the bottom and extending the width of the tank as divided.

For the N-series runs, the experimental reservoir was first filled with layers of water containing appropriate quantities of salt (NaCl) to give a linear gradient of density from top to bottom. This water was then allowed to stand overnight or about 15 h so that the density distribution would become smoothly linear by molecular diffusion. The next morning the density profile was measured indirectly by measuring the electrical conductivity of the solution at various levels in the reservoir. A typical density profile is shown in figure 7. The discharge valve was then opened and the flow rate regulated. After waiting about 5–10 min

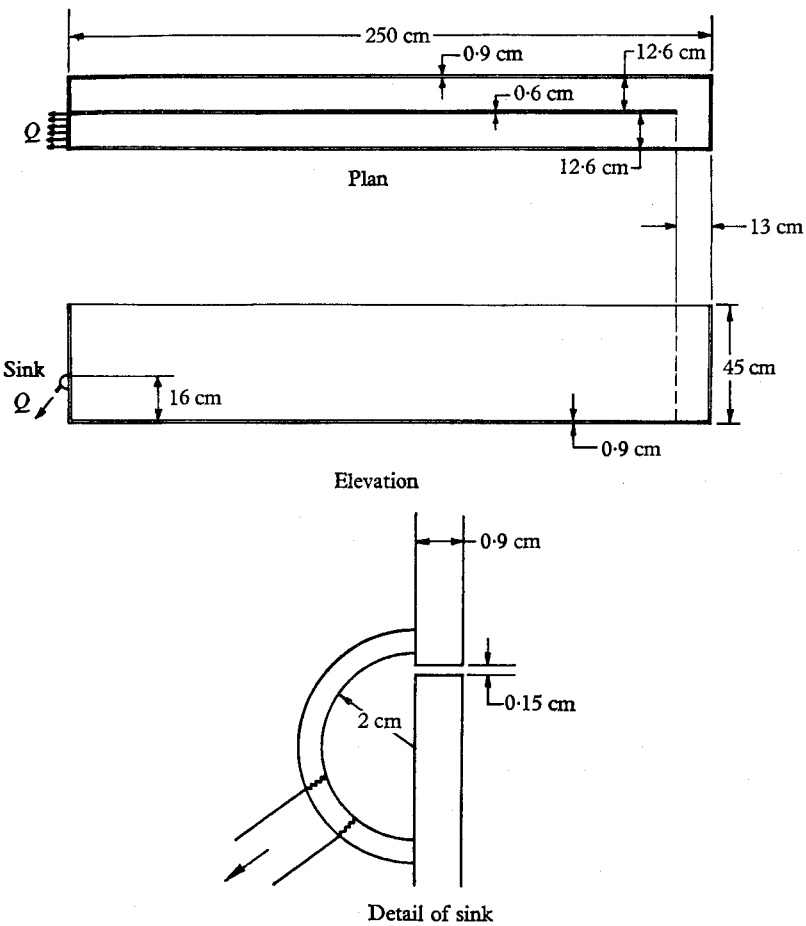

FIGURE 6. Schematic drawing of the experimental reservoir.

for the system to reach a quasi-steady state, dye particles were dropped into the reservoir at different stations upstream of the slit. As the dye particles fell, they left distinct vertical traces. Photographs were taken at time intervals so that the horizontal motions of the dye lines were recorded intermittently. Portions of typical photographs are shown in figure 8 (plate 1). Approximately 10 min after the first set of dye particles were introduced, a second set was introduced in the same way and photographs taken as before. At the end of the experiments, the discharge valve was shut off and the remaining liquid in the reservoir saved.

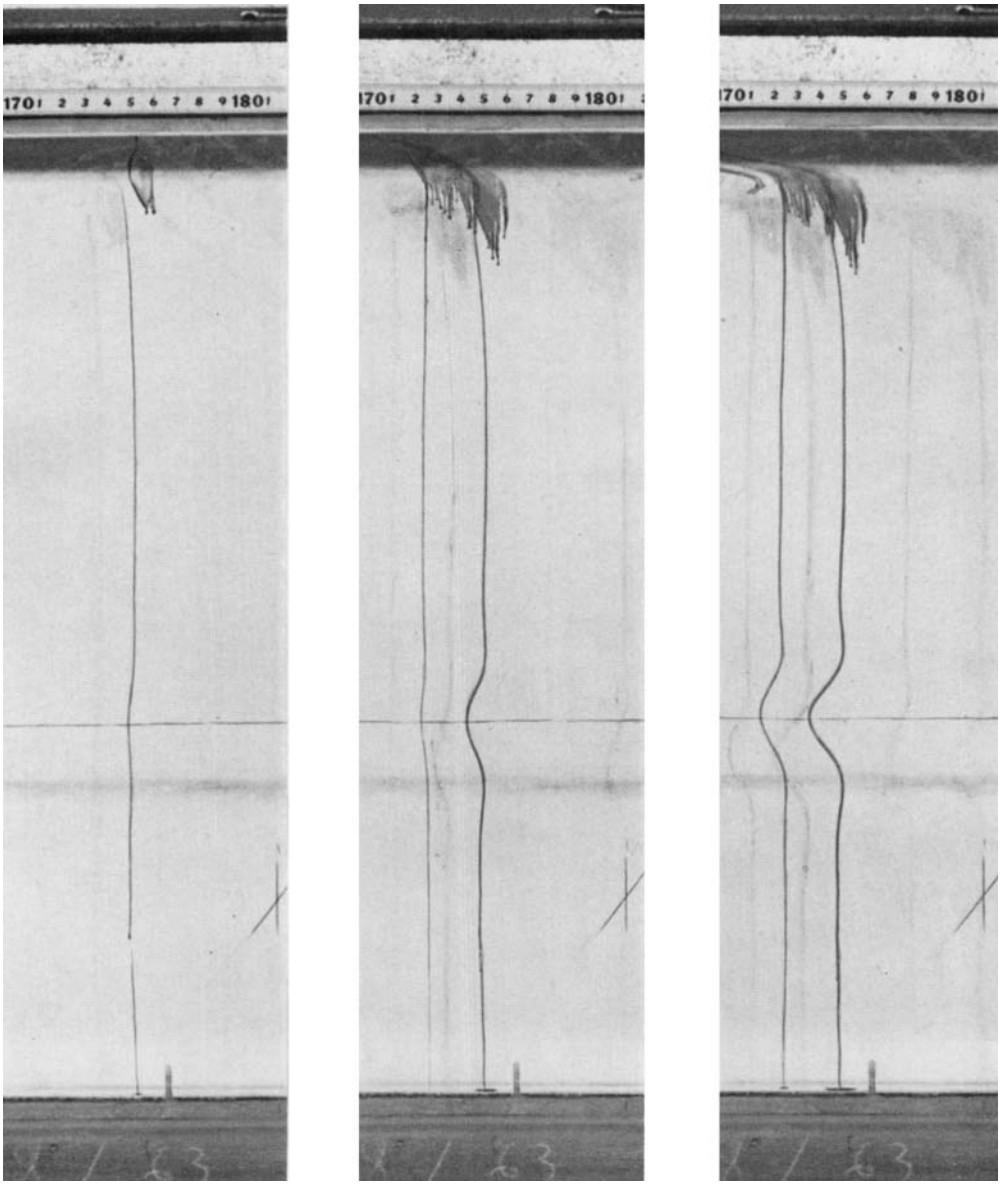

(*a*) (*b*) (*c*)

FIGURE 8. Typical time lapse photographs of dye lines (run N–50–0·5). (*a*) Dye line at time t_0. (*b*) Dye lines at time $t_0 + 55$ sec. (*c*) Dye lines at time $t_0 + 110$ sec.

After the dye had disappeared by diffusion (about 24 h) a density profile was taken again and another experiment could be performed with the remaining liquid at a different flow rate. For each filling of the reservoir, three experiments were performed. After that, the colour of the water became so blue from the dye that no further dye streaks could be readily distinguished.

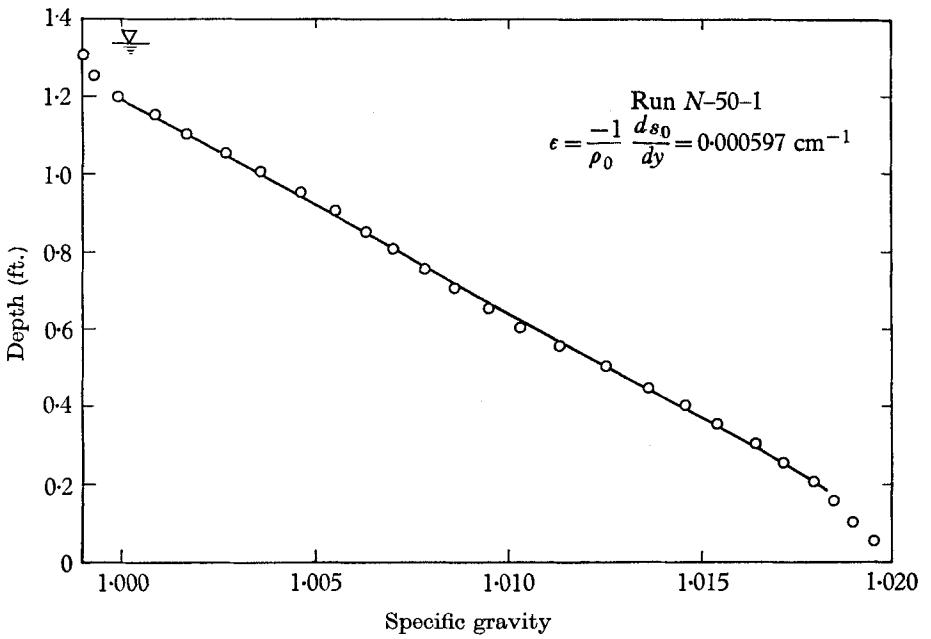

FIGURE 7. Typical measured density profile.

For the T-series runs, the reservoir was filled with layers of water at appropriately varying temperatures. A temperature profile was then measured with a thermomemter and the experiment was performed immediately in the same way as for the N-series runs. In the T-series, only one experiment was performed for each filling of the reservoir.

The discharge was measured volumetrically for both series. Velocity profiles were measured from displacements of the vertical dye lines on photographs taken at different times (figure 8, plate 1). The photographs were superposed in the dark-room and the dye lines traced, from which displacements can be easily measured.

A summary of the experimental parameters is presented in table 1.

2.2. *Measurement and calculation of data from velocity profiles*

Besides the basic measured quantities listed in table 1 and the velocity profiles discussed in the next section, the following parameters were measured from selected dye traces (refer to figure 9):

(i) x(cm), the distance of the dye traces from the sink.

(ii) $u_{\max}(x)$ (cm/sec), the maximum horizontal velocity on a vertical profile at distance x. This is found to be always along the level of the sink.

(iii) $y_0(x)$ (cm), half the thickness of the withdrawal layer as measured by the intersection of the dye images. This measurement is not very accurate since it is

strongly influenced by any mis-alignment in the process of superposition of the dye images.

(iv) $q_f(x)$ (cm²/sec), the forward-flowing unit discharge as measured by the area enclosed by the dye images. Throughout the calculations leading to the experimental results the measured local unit forward discharge q_f has been used

Run	Density gradient, $\epsilon = \frac{-1}{\rho_0}\frac{ds_0}{dy}$ (10^{-5} cm^{-1})	Unit discharge measured at outlet, q (cm²/sec)	Diffusivity, D (10^{-5} cm²/sec)	Kinematic viscosity, ν (10^{-5} cm²/sec)	Temp., T (°C)	Depth, d (cm)	α_0 (cm$^{-\frac{1}{3}}$)
N-8-1·7	7·35	0·127	1·25	900	25·0	43·8	9·13
N-8-3·5	6·76	0·271	1·25	900	25·1	43·4	9·0
N-8-11·7	6·76	0·904	1·25	900	25·1	43·0	9·0
N-12-0·15	12·8	0·0108	1·25	950	22·5	41·3	10·0
N-12-0·3	12·8	0·0232	1·25	950	22·5	41·8	10·0
N-12-0·9	12·8	0·0723	1·25	970	21·5	41·0	10·0
N-12-2·3	14·4	0·179	1·25	950	22·5	41·2	10·2
N-12-4·4	14·4	0·335	1·25	960	22·0	40·6	10·2
N-12-10	14·4	0·760	1·25	960	22·0	40·5	10·2
N-25-0·04	29·5	0·0032	1·25	960	22·0	41·4	11·5
N-25-0·2	26·0	0·0153	1·25	960	22·0	41·5	11·3
N-25-0·5	28·9	0·0392	1·25	960	22·0	41·6	11·5
N-25-1·5	26·2	0·121	1·25	960	21·8	42·6	11·3
N-25-5	25·6	0·412	1·25	960	22·0	43·7	11·2
N-25-9	25·9	0·710	1·25	960	22·0	42·0	11·4
N-50-0·13	59·7	0·0100	1·25	950	23·0	41·3	13·0
N-50-0·5	59·7	0·0376	1·25	950	23·0	41·5	13·0
N-50-1	59·7	0·0727	1·25	950	22·5	40·8	13·0
N-50-3	57·0	0·245	1·25	960	22·0	41·6	12·9
N-50-6	67·4	0·474	1·25	960	22·0	39·7	13·2
N-50-11·7	63·0	0·896	1·25	960	22·0	40·0	13·1
T-16-0·6	16·4	0·0485	144–149	700–880	26·0–37·0	39·7	4·91
T-18-2·0	18·2	0·154	144–149	690–890	25·5–38·0	39·7	5·00
T-21-2·4	20·9	0·188	144–150	660–890	25·5–40·0	39·7	5·15
T-10-5	9·5	0·388	144–147	760–930	23.6–32·8	41·0	4·45

TABLE 1. Summary of basic experimental parameters for each run

instead of the average unit discharge q, measured at the outlet. The finiteness of the tank in length and width is the primary reason for this choice. Thus q was never used in the calculation of any experimental result.

To facilitate comparison between the experimental result and the analytical solution, the same change of q to q_f may be accomplished in the analytical solution. From the numerical analysis it has been found that (see also figure 4)

$$\left(\frac{q_f}{q}\right)_{\text{theory}} = \frac{f_0(3{\cdot}57)}{f_0(\infty)} = \frac{0{\cdot}531}{0{\cdot}500} = 1{\cdot}06. \tag{2.1}$$

2.3. *Similarity in the velocity profiles*

A number of velocity profiles were measured for each experiment. These velocity profiles were for various distances upstream, i.e. various values of x. From the experimental observations, it was noted that there was similarity among these

velocity profiles; in other words, when the velocity profiles were plotted in the form $u/u_{\max}$ against $y/\bar{y}_0$, the curves were the same for all the runs and all the values of x except those very near the sink. Here $u_{\max}$ is the maximum velocity which was found to be always at the level of the sink and $\bar{y}_0$ is defined to be

$$\bar{y}_0 = \frac{q_f}{|u_{\max}|}(0{\cdot}955), \tag{2.2}$$

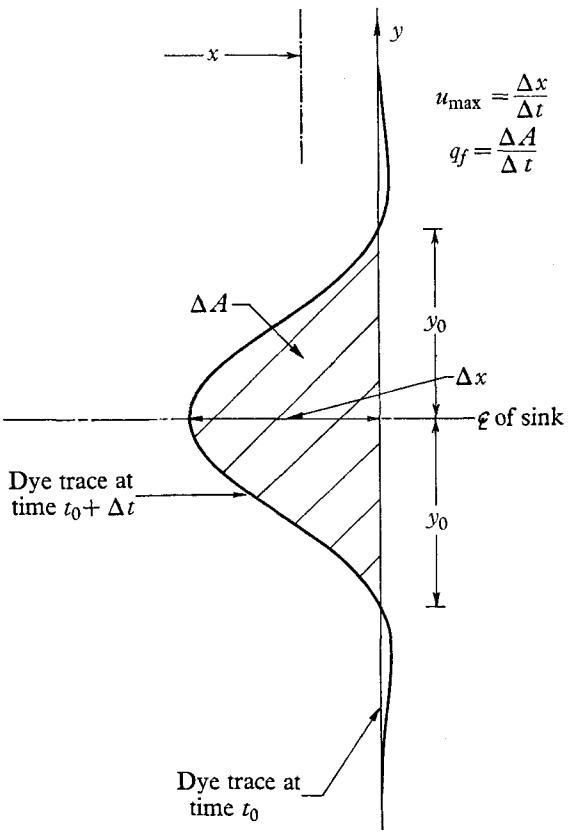

FIGURE 9. Definition sketch.

where q_f is the forward-flowing unit discharge; and the factor 0·955 is used to facilitate comparison with theory. In plotting the data this way, all the velocity profiles pass through the point $u/u_{\max} = 1$ at $y/\bar{y}_0 = 0$. Also, in defining $\bar{y}_0$ by equation (2.2), the area under the curve from $y = 0$ to the point where $u/u_{\max}$ crosses the $y/\bar{y}_0$ axis is forced to be constant, since

$$\int_0^{y=y_0} \frac{u}{u_{\max}} d\left(\frac{y}{\bar{y}_0}\right) = \int_0^{y_0} \frac{u\,dy}{0{\cdot}955 q_f} = \frac{1}{2(0{\cdot}955)}.$$

The purpose of the dimensionless velocity graphs in figure 10 chosen as a representative group from the 25 available is to demonstrate the similarity in the shape of the velocity profiles for the various experiments. Approximately three to five profiles were selected at random from each experiment and plotted

in this way. This similarity in the velocity profiles is one of the most significant results of the experiments.

Although strictly speaking the analytical solution for the velocity distribution should not be applied to the majority of the experiments, it may nevertheless be represented in the form $u/u_{\max}$ against $y/\bar{y}_0$. In fact the number 0·955 in the definition of $\bar{y}_0$ in equation (2.2) was so chosen that the analytical solution represented in that same way, would pass through the point $u/u_{\max} = 0$ at $y/\bar{y}_0 = 1$. As a comparison, the analytical solution has been drawn in figure 10

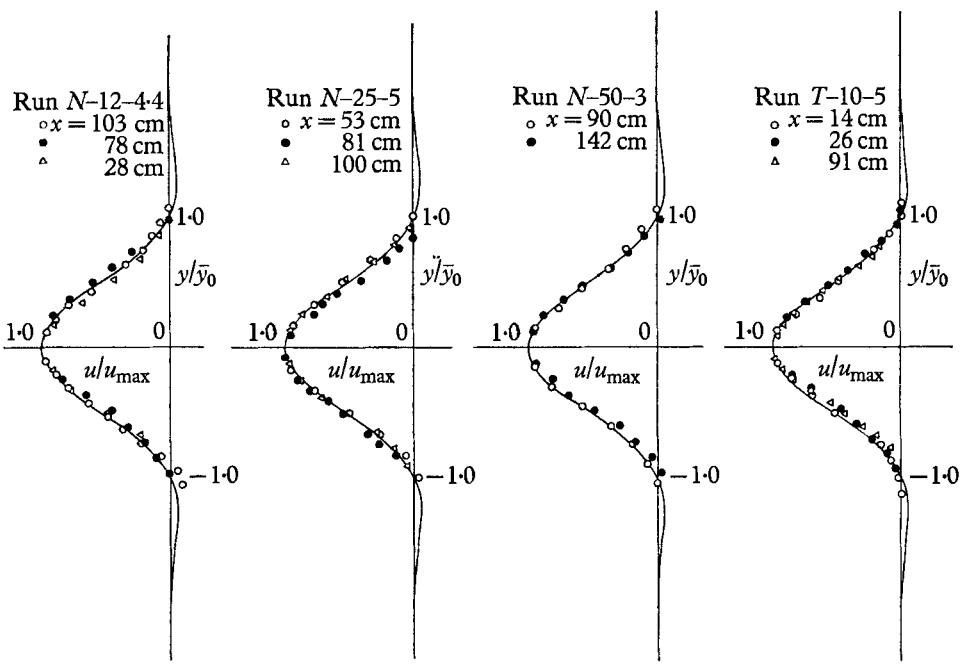

FIGURE 10. Velocity profiles for various runs.

as solid lines. It is readily seen that as far as the shape of the velocity profiles is concerned, the experimental results fit the shape of the analytical profile extremely well even though the experiments were not all carried out for the values of $\epsilon\delta$, δ/x, $q/D\alpha_0 x^{\frac{3}{2}}$, and $q/\nu\alpha_0 x^{\frac{3}{2}}$ small compared to 1 as required by the theory.

From these graphs it may therefore be concluded that the shape of the velocity profiles $u(y)$, obtained from the experiments, is the same as that predicted by the analysis presented in § 1.

2.4. *An extension of the zeroth-order solution*

In § 2.3 (equation (2.2)), $\bar{y}_0$ was defined to be a length by which the vertical co-ordinate y was normalized so that the area under the curve would be constant. But there is another way that this length $\bar{y}_0$ may be interpreted which will have direct bearing on the conclusions which will be drawn from these experiments later.

In the zeroth-order solution obtained in § 1, the principal result is

$$u(x,y) = \frac{\alpha_0 q}{x^{\frac{1}{3}}} f_0'\left(\frac{\alpha_0 y}{x^{\frac{1}{3}}}\right), \tag{2.3}$$

where, as defined before, $\alpha_0 = (\epsilon g/D\nu)^{\frac{1}{6}}$. The function $f_0(\zeta)$ is illustrated graphically in § 1 (figure 4). $f_0'(\zeta)$ is symmetrical about $\zeta = 0$ and hence

$$u_{\max} = \frac{\alpha_0 q}{x^{\frac{1}{3}}} f_0'(0) = -0{\cdot}284\,\frac{\alpha_0 q}{x^{\frac{1}{3}}}, \tag{2.4}$$

where the number $-0{\cdot}284$ is the value of $f_0'(0)$ as obtained in § 1. In terms of q_f (as defined by equation (2.1)), equation (2.4) may be rewritten

$$u_{\max} = -0{\cdot}267\alpha_0 q_f/x^{\frac{1}{3}}. \tag{2.5}$$

Now in equation (2.5), the only quantity which is not kinematic is α_0. The kinematic quantities $u_{\max}$, q_f, and x may very simply be measured in the dye traces. Let one postulate that in cases when $q/D\alpha_0 x^{\frac{2}{3}}$ is no longer small, the same zeroth-order solution may be applied provided one replaces α_0 with a variable parameter α. Hence define $\chi = \alpha/\alpha_0$ where α is the value obtained from the experimental velocity profiles. Then

$$\chi = \alpha/\alpha_0 = \left\{\frac{|u_{\max}|\, x^{\frac{1}{3}}}{\alpha_0 q_f(0{\cdot}267)}\right\}_{\text{measured}} \tag{2.6}$$

There is, however, another way of obtaining χ, this time based on y_0, which is half the thickness of the withdrawal layer as measured from the dye lines. From the analytical solution in figure 4, for $f_0'(\alpha_0 y_0/x^{\frac{1}{3}}) = 0$, we find that

$$\alpha_0 y_0/x^{\frac{1}{3}} = 3{\cdot}57. \tag{2.7}$$

Now y_0 and x may be measured and another χ may be computed by the formula

$$\chi' = \alpha'/\alpha_0 = \left\{\frac{3{\cdot}57x^{\frac{1}{3}}}{\alpha_0 y_0}\right\}_{\text{measured}} \tag{2.8}$$

It turns out that $\chi = \chi'$ and $y_0 = \bar{y}_0$ within experimental error. Thus, the zeroth-order solution may be applied in all the cases obtained in the experiments provided one uses the appropriate value of α.

2.5. *The experimental parameter* $\chi = \alpha/\alpha_0$

As explained in the previous sections, and as may be seen in figure 10, the zeroth-order solution obtained in § 1 is remarkably accurate provided the value of α_0 is replaced by α, even though $q/D\alpha_0 x^{\frac{2}{3}}$ and $q/\nu\alpha_0 x^{\frac{2}{3}}$ are no longer small. It is therefore of the utmost importance to investigate how the value $\chi = \alpha/\alpha_0$ is related to the other physical parameters since once χ is known, the flow field is known. From dimensional analysis one expects

$$\chi = \text{function}\left\{\frac{q}{D\alpha_0 x^{\frac{2}{3}}}, \frac{D}{\nu}, \epsilon\delta, \delta/x\right\}.$$

Since $\epsilon\delta$ and δ/x are indeed quite small as assumed in the theoretical solution, one expects the dependence of χ on them to be small. Of course, when all these four

parameters are small, one expects χ to be unity. The value χ as computed using the equation (2.6) was plotted against the variable $q_f/D\alpha_0 x^{\frac{2}{3}}$. For each of the experiments separately they are as shown in figures 11 and 12, where a representative group are given. A straight line is drawn through each group of points and these lines are compiled in figure 13. The points representing the T-series

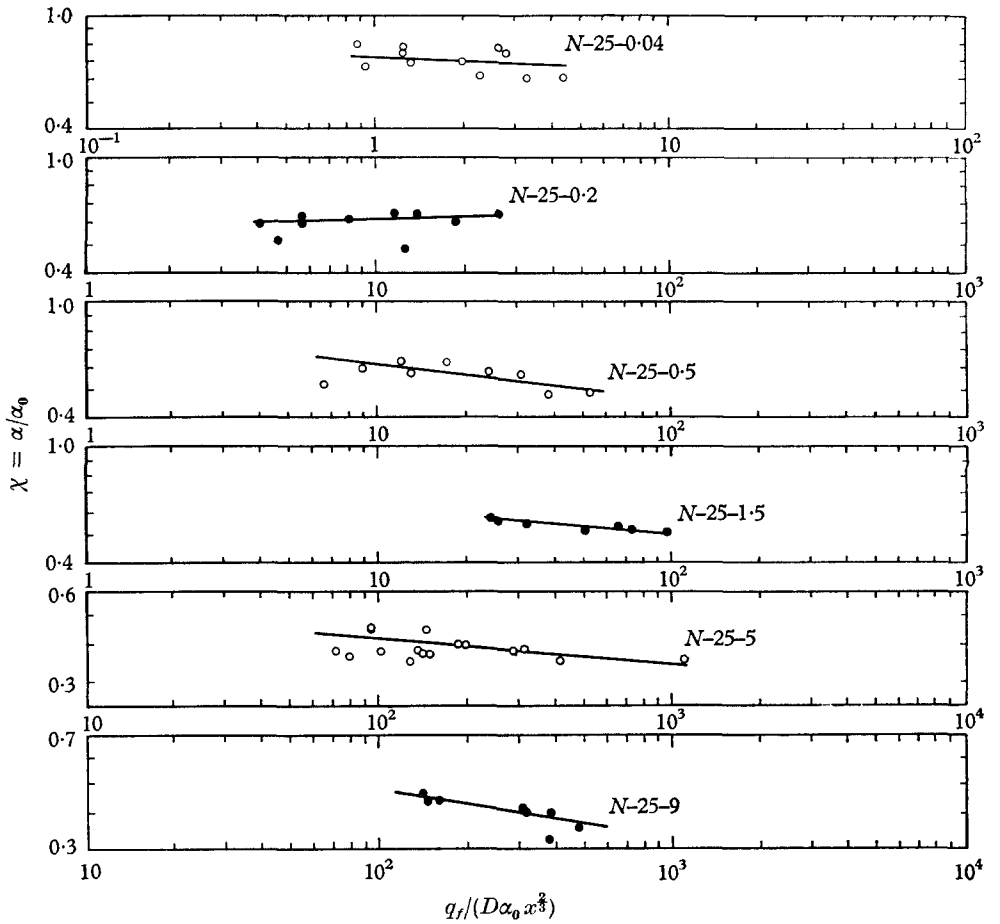

FIGURE 11. Variation of $\chi = \alpha/\alpha_0$ with $q_f/(D\alpha_0 x^{\frac{2}{3}})$ for the N–25-series runs.

runs are slightly displaced from those of the N-series runs. This is because the quantity D/ν was $1{\cdot}25 \times 10^{-3}$ for the N-series runs and 0·150 for the T-series runs. However, this displacement is not very large and is in fact within the experimental scatter. The experimental scatter may be attributed to several causes which will be described and discussed in the next section.

2.6. *Summary of experimental errors*

The apparatus was constructed to simulate the case of steady linearly stratified, two-dimensional flow into a hydrodynamic sink. Because of the finite width of the tank, the flow was not two-dimensional. Because of the finite length, the

flow was not steady and the discharge not constant with respect to x. All these effects were investigated with regard to the amount of systematic error they produce. Since the locally measured forward-flowing discharge q_f is used in all the computations of the experimental results instead of the discharge measured at the outlet q, it is believed that these errors do not amount to more than 10 %.

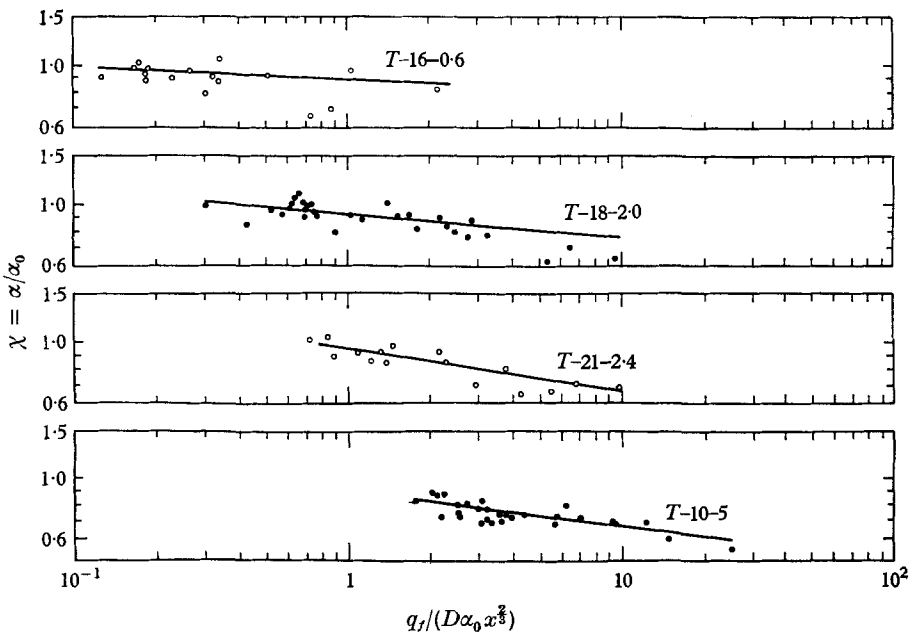

FIGURE 12. Variation of $\chi = \alpha/\alpha_0$ with $q_f/(D\alpha_0 x^{\frac{2}{3}})$ for the T-series runs.

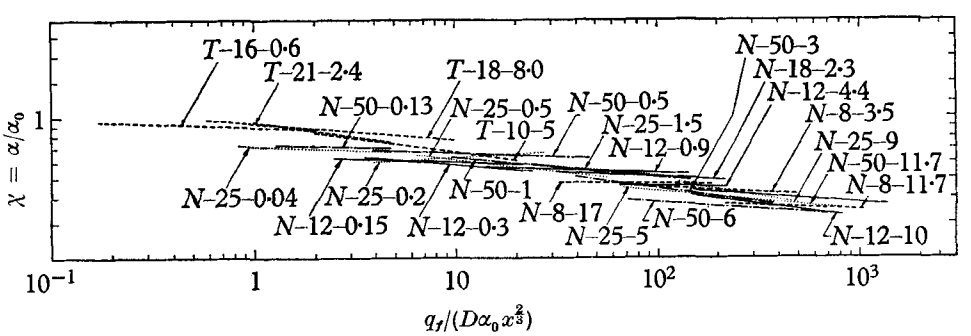

FIGURE 13. Variation of $\chi = \alpha/\alpha_0$ with $q_f/(D\alpha_0 x^{\frac{2}{3}})$.

The most significant errors should be in x-dependent results since most of the error-producing items such as the length effect are x-dependent. Besides these systematic errors, there are, of course, random errors. A few of the more important ones will now be discussed.

In the measurements of the velocities by means of the dye traces the steps involved included the tracing of images from the negatives on to the paper. In so doing, the various images must first be aligned with the aid of various reference

crosses on the front side of the tank. Then the scale of the photograph had to be established by matching the scale in the photograph on the front side of the tank with a scale in the darkroom. Moreover, the distance in from the wall to various dye streaks was slightly variable making slight errors in the photographically measured lengths. It is believed that these errors, together with the systematic errors discussed earlier, are the cause of the scatter shown in figures 11 and 12 (roughly 15 %).

2.7. *Conclusion*

Theoretical studies of incompressible, steady, viscous flow towards a sink in a stably stratified fluid were made. Both the two-dimensional and the axisymmetric cases were treated. Experiments on the two-dimensional case were also performed. The major conclusions can be summarized as follows:

(1) The limiting solutions applicable for very small discharge were obtained analytically by first making a boundary-layer-type assumption and then a perturbation based on the parameters $q/D\alpha_0 x^{\frac{2}{3}}$ or $Q/2\pi D\alpha_0 x^{\frac{5}{3}}$. They are similarity-type solutions, based on the similarity variable

$$\zeta = \alpha_0 y/x^{\frac{1}{3}} \quad \text{or} \quad \alpha_0 z/r^{\frac{1}{3}}.$$

These solutions are presented in § 1.

(2) According to these solutions, the thickness of the withdrawal layer grows with distance x (or r) upstream like $x^{\frac{1}{3}}$ (or $r^{\frac{1}{3}}$) and is inversely proportional to the parameter $\alpha_0 = (\epsilon g/D\nu)^{\frac{1}{6}}$; the equations for δ are for the two-dimensional case, $\delta = 7{\cdot}14x^{\frac{1}{3}}/\alpha_0$ and for the axisymmetric case $\delta = 5{\cdot}8r^{\frac{1}{3}}/\alpha_0$.

(3) Also, according to these solutions, the velocity field for the two-dimensional case is given by

$$u(x, y) = \frac{\alpha_0 q}{x^{\frac{1}{3}}} f_0'\left(\frac{\alpha_0 y}{x^{\frac{1}{3}}}\right),$$

where $f_0'(\zeta)$ is shown graphically in figure 4 (*a*). For $y = 0$,

$$u = u_{\max} = -0{\cdot}284\alpha_0 q/x^{\frac{1}{3}}.$$

For the axisymmetric case,

$$u(r, z) = \frac{\alpha_0 Q}{2\pi r^{\frac{4}{3}}} f_0'\left(\frac{\alpha_0 z}{r^{\frac{1}{3}}}\right),$$

where this $f_0'(\zeta)$ is shown graphically in figure 5 (*a*). For $z = 0$,

$$u = u_{\max} = -0{\cdot}35\alpha_0 Q/2\pi r^{\frac{4}{3}}.$$

(4) Twenty-five experiments were carried out to simulate the two-dimensional case where the range of variation of the parameter $q_f/D\alpha_0 x^{\frac{2}{3}}$ was 10^{-1} to 10^3. It was found that within the region of applicability of the analytical solution ($q_f/D\alpha_0 x^{\frac{2}{3}} < 1$ in the experiments), the experimentally determined velocity profiles agree within 10 % with the analytical.

(5) However, outside the range of direct applicability of the analytical solution, ($1 < q_f/D\alpha_0 x^{\frac{2}{3}} < 10^3$ in the experiments), experimental observations show that the shape of the velocity profile is still the same as predicted. By

varying α_0 to α by means of an experimentally determined coefficient $\chi = \alpha/\alpha_0$, these experimental results may also be made to fit the equations of the analytical solution. The coefficient was found to be a function of $q_f/D\alpha_0 x^{\frac{2}{3}}$ as given in figure 13. No experiments have as yet been done on the axisymmetric case.

(6) For all the experiments, the local velocity profiles are similar in the sense that $u/u_{\max} = f(y/\bar{y}_0)$.

(7) For all the experiments, the formula for $\delta(x)$ is

$$\delta(x) = 7{\cdot}14x^{\frac{1}{3}}/\alpha,$$

where $\alpha(x) = \chi\alpha_0$ (figure 13).

In closing, the author wishes to thank Prof. Norman H. Brooks as well as other members of his committee for many valuable suggestions and criticisms. The work was supported in part by the National Institute of Health, U.S. Public Health Service under Grant no. WP-00428.

REFERENCES

DEBLER, W. R. 1959 Stratified flow into a line sink. *Proc. Am. Soc. Civ. Engrs., J. Engrng Mech. Div.*, no. EM3, **85**, 51–65.

GARIEL, P. 1949 Experimental research on the flow of non-homogeneous fluids. *La Houille Blanche*, pp. 56–64.

KAO, T. W. 1963 The phenomenon of blocking in stratified flow. Ph.D. thesis, University of Michigan.

KOH, R. C. Y. 1964 Viscous stratified flow towards a line sink. Ph.D. thesis, California Institute of Technology.

LONG, R. R. 1962 Velocity concentrations in stratified fluids. *Proc. Am. Soc. Civ. Engrs., J. Hydr. Div.*, no. HY 1, **88**, 9–26.

YIH, C. S. 1958 On the flow of a stratified fluid. *Proc. Third Nat. Congr. Appl. Mech.*